Petroleum Science 21 (2024) 2080–2088

Contents lists available at ScienceDirect

Petroleum Science

journal homepage: www.keaipublishing.com/en/journals/petroleum-science

Original Paper

Experimental study on wax deposition of highly paraffinic oil in intermittent gas-oil flow in pipelines

Chuan-Shuo Wang [a], Qian-Li Ma [a], Xiao-Fang Lv [a, *], Jie Zhang [b], Yang Liu [a, **], Shi-Dong Zhou [a]

[a] Jiangsu Key Laboratory of Oil and Gas Storage and Transportation Technology, Changzhou University, Changzhou, 213164, Jiangsu, PR China
[b] Hade Oil and Gas Development Department, Tarim Oilfield Branch, Korla, 841000, Xinjiang, PR China

ARTICLE INFO

Article history:
Received 22 March 2023
Received in revised form
2 January 2024
Accepted 3 January 2024
Available online 7 January 2024

Edited by Jia-Jia Fei

Keywords:
Oil-gas two phase
Highly paraffinic oil
Wax deposition
SAXS

ABSTRACT

Oil-gas two phase wax deposition is a fairly common and open-ended question in flow assurance of multiphase transportation pipelines. This paper investigated the two main aspects of oil-gas two phase wax deposition layer: apparent thickness and crystal structure characteristics. A typical highly paraffinic oil in Bohai Sea, China, was used as the experimental material to investigate the wax deposition thickness in oil-gas two phase under the influence of different oil temperatures, superficial gas/liquid phase velocities and gas-oil ratios by using multiphase flow loop experimental device. Just as in the classical theory of wax molecular diffusion, it showed that wax deposition thickness of oil-gas two phase increased with increasing oil temperature. Analysis of the impact of different superficial phase velocities found that the actual liquid flow heat transfer and shear stripping was the gas phase dominant mechanisms determining wax deposit thickness. In addition, the crystal structure of the wax deposition layer was characterized with the help of small-angle X-ray scattering (SAXS) for different circumferential positions, flow rates and gas-oil ratios. The bottom deposition layer had a complex crystal structure and high hardness, which were subject to change over flow rate variations. Furthermore, the SAXS results provided evidence that the indirect effect of the actual liquid velocity modified by the gas phase was the main mechanism. Our study of the effect of gas phase on the wax deposition of oil-gas two phase will help shed light onto the mechanism by which this important process occurs. Our findings address a very urgent need in the field of wax deposition of highly paraffinic oil to understand the flow security of oil-gas two phase that occurs easily in multiphase field pipelines.

1. Introduction

The prevalence of multiphase transportation motivated extensive research, which nevertheless did not culminate in a satisfactory understanding of wax deposition in gas-oil two phase flow (Aiyejina et al., 2011; Leporini et al., 2019; Liu et al., 2020). The role that gas phase play in wax deposition is still not fully understood and requires further research. So far, a number of researchers have carried out experimental research on the influence of oil-gas two phase flow patterns on wax deposition (Quan et al., 2018; Yu et al., 2021). Flow loop apparatus was widely used in other seminal work, covering both the stratified flow and the intermittent flow under a wide range of hydraulic and thermal conditions (Duan et al., 2017, 2018; Singh et al., 2017).

Many of the early experiments of oil-gas two phase wax deposition were pioneered in Tulsa University. Matzain et al. (2002) presented experimental results first from the thickness and components of oil and gas two-phase wax deposition under different flow patterns. A definitive understanding of wax deposition characteristics and mechanism for a certain flow type has not yet been reached, being the subject of follow-up research. Rittirong et al. (2017) and Chi et al. (2019) systematically studied the overall and local deposition in circumferential direction under intermittent and stratified flow, respectively. Rittirong et al. (2017) conducted a large group of flow loop tests at a wide variety of superficial gas and liquid velocity. It was shown that the deposit thickness decreased as the superficial liquid velocity (V_{sl}) increased, while the thickness increased as superficial gas velocity (V_{sg}) increased. It turned out

* Corresponding author.
** Corresponding author.
E-mail addresses: lvxiaofang5@cczu.edu.cn (X.-F. Lv), liu.y@cczu.edu.cn (Y. Liu).

https://doi.org/10.1016/j.petsci.2024.01.003

that there were particular crossover points of the obtained results for different superficial gas velocity conditions. The circumferential direction results indicated that the wax deposit layer on the top was thicker and softer than those on the bottom, as a result of the difference between gas and liquid phase shear stress. By pressurized multiphase flow loop, Chi et al. (2019) obtained wax deposition data for oil-gas two phase stratified flow at different liquid and gas flow rates. It has been shown that deposition mass and wax content increased with increasing superficial gas or liquid velocity. The primary reason for the increase of wax content and deposit mass was to increase the actual liquid velocity, enhancing the convective heat transfer increase. Further, the analysis results of local deposit components exhibited that the influence of superficial gas or liquid velocity on the side deposition was greater than that on the bottom. The proportion of high carbon number fraction increased with increasing superficial velocity.

Subsequently, Chinese scholars (Duan et al., 2017, 2018; Gong et al., 2011; Quan et al., 2018, 2020) carried out a series of relevant experiments with highly paraffinic oil. The results of the circumferential distribution of wax deposition layers under stratified and intermittent flow patterns observed by Gong et al. (2011) and Quan et al. (2018, 2020) were similar to those of Matzain et al. (2002). However, there were some differences in the deposition thickness variation patterns at different superficial velocities. This may be related to the differences in their experimental oil samples and experimental condition parameter settings. In terms of the mechanisms, two main gas actions for multiphase wax deposition have been proposed: (i) The “direct gas-phase action” includes flow pattern changes and gas-phase shear stripping action. (ii) The “indirect gas-phase action”, in which the gas phase changes the liquid phase flow, followed by the influence of heat transfer and liquid phase shear stripping. In intermittent gas-liquid flow, Matzain et al. (2002) and Rittirong et al. (2017) noted that the 24-h deposition thickness monotonically decreased with increasing superficial liquid velocity. This was mainly due to high wall shear (high actual liquid phase flow rate). However, Gong's (Gong et al., 2011) and Quan's (Quan et al., 2020) results showed that with the increase of V_{sl}, the 24-h deposition thickness increased first and then decreased. One of the growth trends was triggered by the liquid phase conversion rate promoting convective heat transfer. Of these proposed mechanisms, it was generally regarded that shear force at pipe wall has dominant contributions to the decrease of 24-h deposition thickness as the increase of superficial gas velocity. Although there were several independent experimental results and mechanistic analysis from a number of research teams performing measurements on different kinds of fluids, none provided the wax crystal microstructure information in the deposition layer with the help of small-angle X-ray scattering (SAXS). As an important means of characterizing crystal structure parameters, SAXS has been applied in the study of materials, polymers, and other systems. When X-rays pass through the sample, if there is an area with uneven electron density in the sample, the X-rays will scatter in the small angle area ($2\theta < 5^{\circ}$), which is called small angle X-ray scattering. Currently, only a few scholars have studied the microstructure parameters of wax crystals. Sun et al. (2007) used SAXS to study the changes in the internal microstructure of wax crystals during the heating process of paraffin. Gouze et al. (2019) used SAXS to characterize the particle size distribution and volume fraction of wax crystals during the temperature change process. Huang et al. (2018) explored the mesoscopic characteristic parameters of wax crystal particles, such as shape, size, distribution, and orientation, with nanocomposite pour point depressants.

In this paper, the wax deposition thickness of typical highly paraffinic oil-gas two phase under the effect of different temperatures, superficial gas/liquid phase velocities and gas-oil ratios was studied by using a multiphase flow loop. Combined with the experimental results of oil-gas two phase deposition and the calculation of flow characteristics parameters, we have made progress on the understanding of the gas action in the wax deposition. Furthermore, the wax crystal structure of the deposition layer at different annular positions was characterized by small angle X-ray scattering (SAXS) to systematically elaborate the mechanism of the gas phase. This has important consequences for our understanding of the mechanism of gas phase action in multiphase pipeline transportation.

2. Experimental materials and methods

2.1. Experimental materials

The BZ crude oil used in this paper was characterized by a high wax content (24.3 wt%), medium resin content (10.56 wt%) and high wax appearance temperature (43.25 °C), which belonged to a typical highly paraffinic crude oil. At 20 °C, the density was 884.39 kg/m^3. Other physical parameters, such as viscosity-temperature relationship curve, wax precipitation characteristic curve, carbon number distribution, etc., were shown in the following Figs. 1–3.

2.2. Experimental equipment

The experimental flow loop of oil-gas two phase wax deposition was mainly made of stainless-steel pipe (total length about 25 m, inner diameter 25.4 mm), and contained the test and reference section, screw pump, tank, temperature control system (water bath, insulation) and data acquisition system, etc. It was equipped with flow meters, differential pressure sensors, temperature sensors and data acquisition systems, etc., see Fig. 4 for details, in order to obtain and record key information such as flow rate, temperature and differential pressure in the loop pipeline in real-time. Based on the differential pressure method (Cai and Zhang, 2003; Van der Geest et al., 2018), the average thickness of the wax deposition layer in the test pipe section under different experimental conditions can be calculated.

In the oil-gas two phase loop experimental scheme, 0, 7 (medium) and 15 (high) were selected as the gas-oil ratio experimental conditions with reference to the actual submarine pipeline gas oil ratio range. The experimental gas phase injection process: air compressor - filter - regulator - gas flow controller. The gas-oil ratio

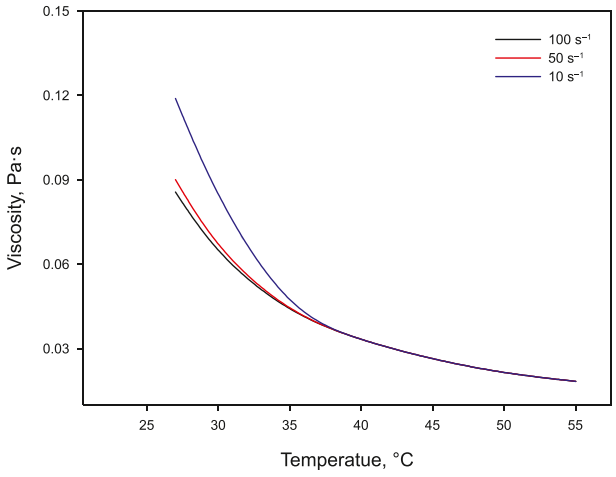

Fig. 1. Viscosity of BZ crude oil.

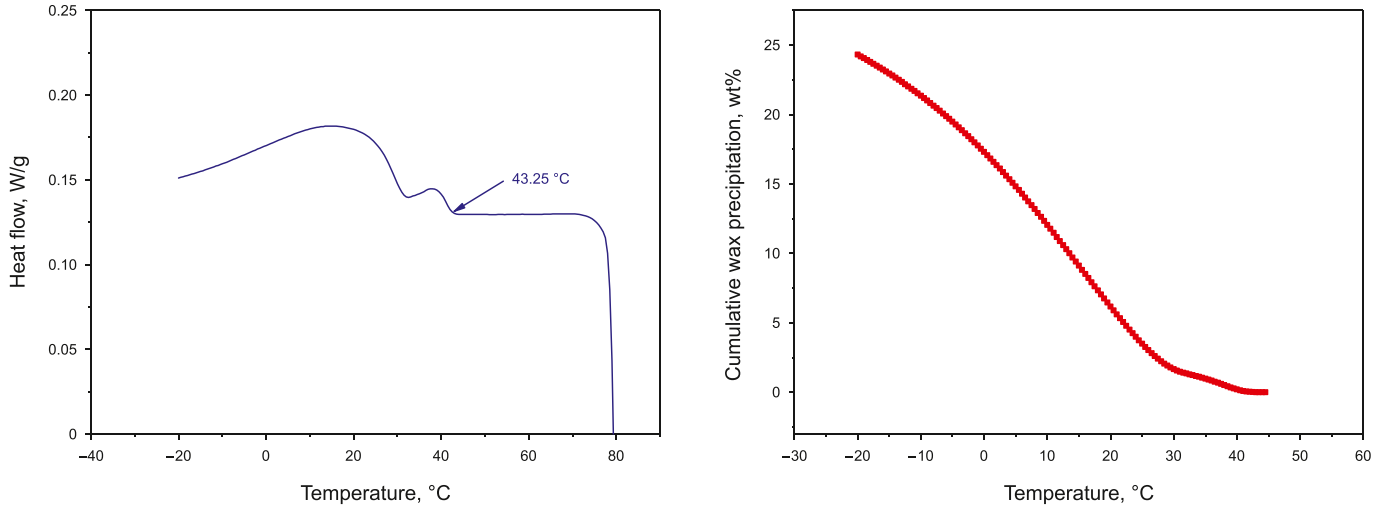

Fig. 2. Wax precipitation characteristics of BZ crude oil.

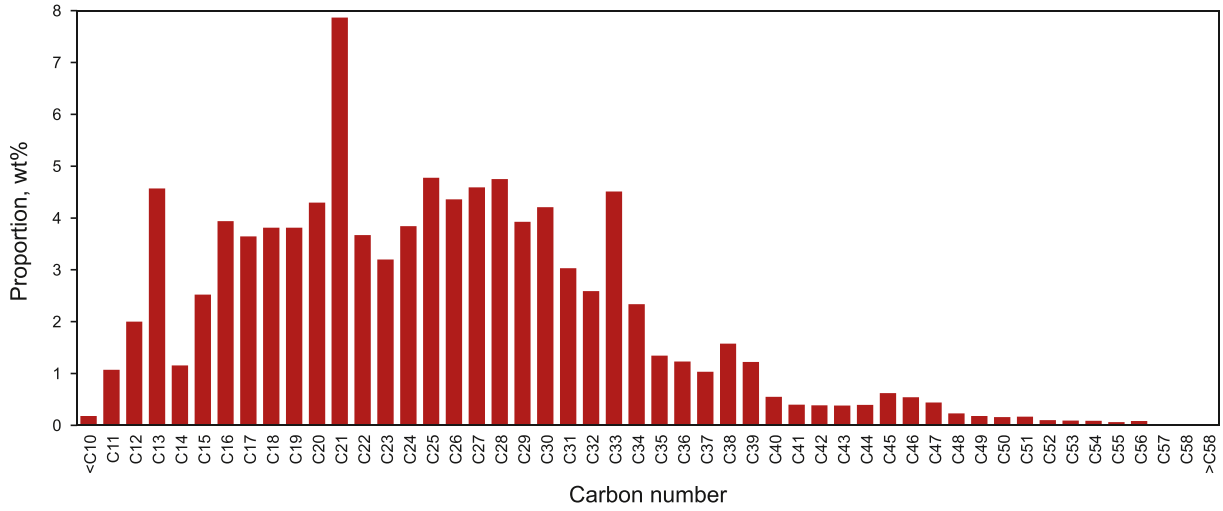

Fig. 3. Carbon number distribution of BZ crude oil.

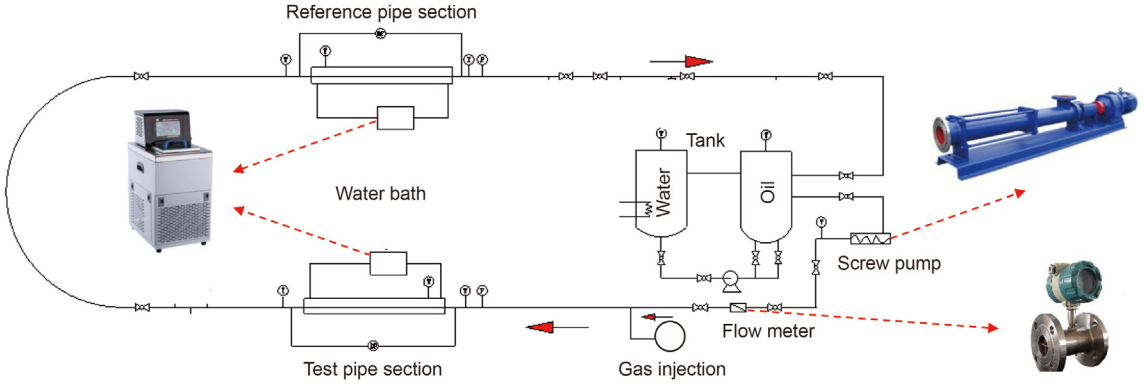

Fig. 4. Flow loop experimental device.

setting was achieved by adjusting the gas phase flow rate during the experiment, which was controlled by the regulator and controller. Of the hydrothermal parameters, the initial inner wall temperature of flow loop was 30 °C (wax appearance temperature = 43.25 °C), and the oil temperature included 40, 45 and 50 °C. The three flow velocities v = 0.8, 1.2 and 1.6 m/s correspond to low velocity laminar, high velocity laminar and turbulent flows, respectively. Deposition time settings of 1, 3, 6, 9, 12 h.

To characterize the wax crystal structure parameters at different annular positions in the deposition layer, a test analysis was performed with the help of a Beijing 1W2A small-angle X-ray scattering device (Dong et al., 1997; Li et al., 2014, 2019). This device mainly consisted of a light source, small-angle camera, detector and other components. Mar165-CCD detector was spaced 1500 mm from the sample, and the sample temperature was controlled by a liquid nitrogen and heating plate. The sample loading process was as follows: SAXS carrier (hollow, approximately 1 mm thick steel plate) filmed on one side. Appropriate amount of wax deposition sample was taken and placed on the membrane to fill the hollow area, and finally the membrane was sealed. After the sample was loaded, it was cooled down to the wall temperature at the same controlled temperature rate, and the constant temperature was waited for 10 min before starting to shoot. The scattering vector $q = 1.67\ \mathrm{nm}^{-1}$, exposure time 100 s, and Fit 2D software were used to process and analyze the experimental data.

3. Results and discussion

The remainder of the article is organized as follows. In Section 3.1, we describe the experimental results of wax deposition in the loop. We then present results first from the small angle X-ray scattering (SAXS) experiments in Section 3.2.

3.1. Wax deposition thickness of flow loop under different influencing factors

The experimental results of wax deposition of highly paraffinic crude oil at different temperatures, flow rates, gas-oil ratios and time were obtained by oil-gas two phase wax deposition loop experiments, and the detailed experimental results were summarized in Supporting information A.

From the above Fig. 5, it could be seen that the deposition thickness of oil-gas two phase increased with the increase of oil temperature/temperature difference between oil temperature and wall temperature under the same flow rate and gas-oil ratio. For example, at low velocity laminar flow and medium gas-oil ratio, the deposition thickness was 0.89 mm after 12-h operation at 40 °C oil temperature. When the oil temperature increased to 45 and 50 °C, the 12-h deposition thickness grew to 1.14 and 1.58 mm, respectively. Similar results hold for other flow patterns/flow rates and deposition time. These observations of wax deposition characteristics at different temperatures were consistent with prior studies (Fan et al., 2021; Singh et al., 2000) showing that molecular diffusion was a control mechanism for oil-gas two phase wax deposition.

Analysis of experimental results of wax deposition at different superficial phase velocities presented can provide insights to further research. The experimental properties of wax deposition at superficial gas/liquid phase velocities were summarized below and the results were shown in Fig. 6.

At the same superficial liquid phase velocity, the wax deposition thickness increased with increasing superficial gas phase velocity at each deposition time. At $V_{sl} = 1.1$ m/s, the superficial gas phase velocity increased from 8.4 to 9.6 m/s, corresponding to the increase of the 12-h average wax deposition thickness from 1.14 to 1.22 mm. Other superficial liquid phase velocity and deposit time conditions were similar to that shown in Fig. 6(a) and (b).

In the analysis of V_{sl}, it was found that the deposition thickness decreased with increasing superficial liquid phase velocity at similar superficial gas phase velocity, as shown in Fig. 6(c) and (d). Under the high superficial gas phase velocity range ($V_{sg} = 9.3$–9.6 m/s), V_{sl} increased from 1.1 to 1.3 m/s and the 12-h wax deposition thickness decreased from 1.22 to 1.04 mm. The

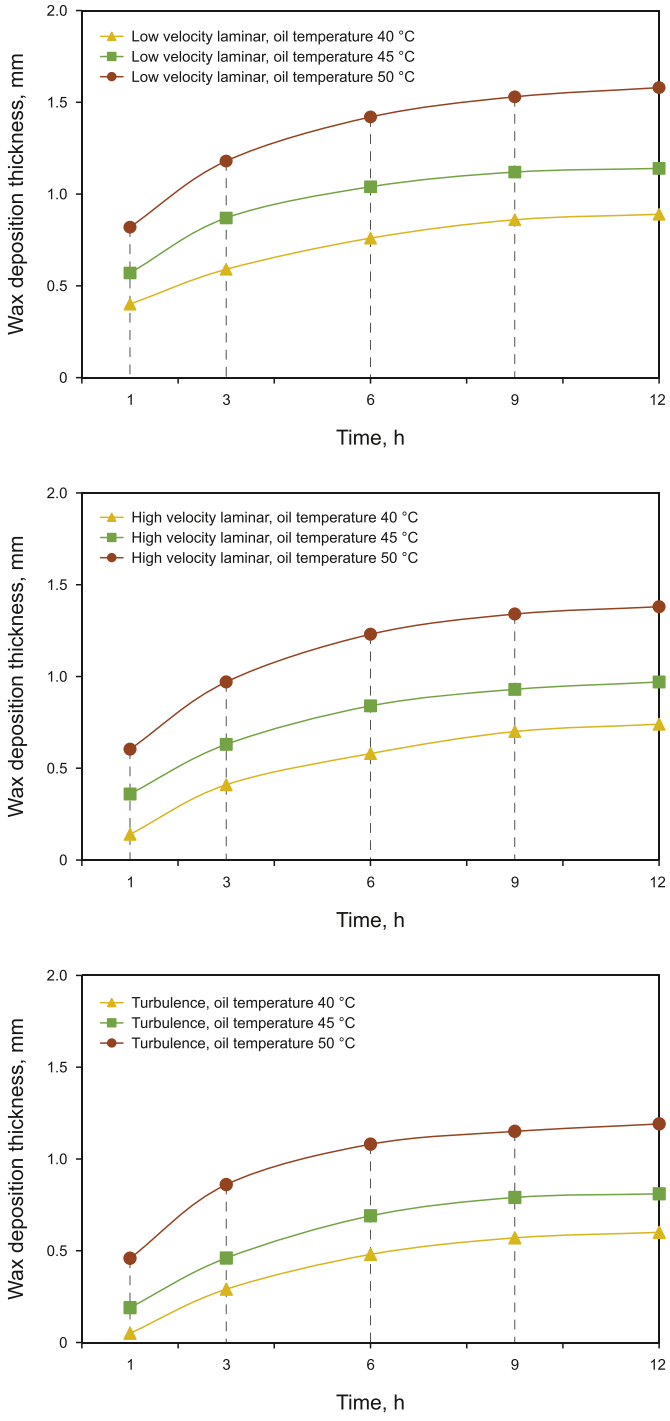

Fig. 5. Wax deposition thickness in oil-gas two phase at different oil temperatures.

12-h wax deposition thickness decreased from 1.58 to 1.38 mm in the range of low superficial gas phase velocity ($V_{sg} = 8.3$–8.4 m/s) with increasing superficial liquid phase velocity.

To get other concrete results and explain the reason behind each section, we calculated the oil-gas two phase flow characteristics parameters, including liquid holdup, actual liquid velocity, and wall shear stress (Zhang and Sarica, 2011). The detailed calculation & result presentation was summarized in Table 1 below.

Based on the molecular diffusion-dominated oil gas two-phase wax deposition framework, an increase in the superficial gas

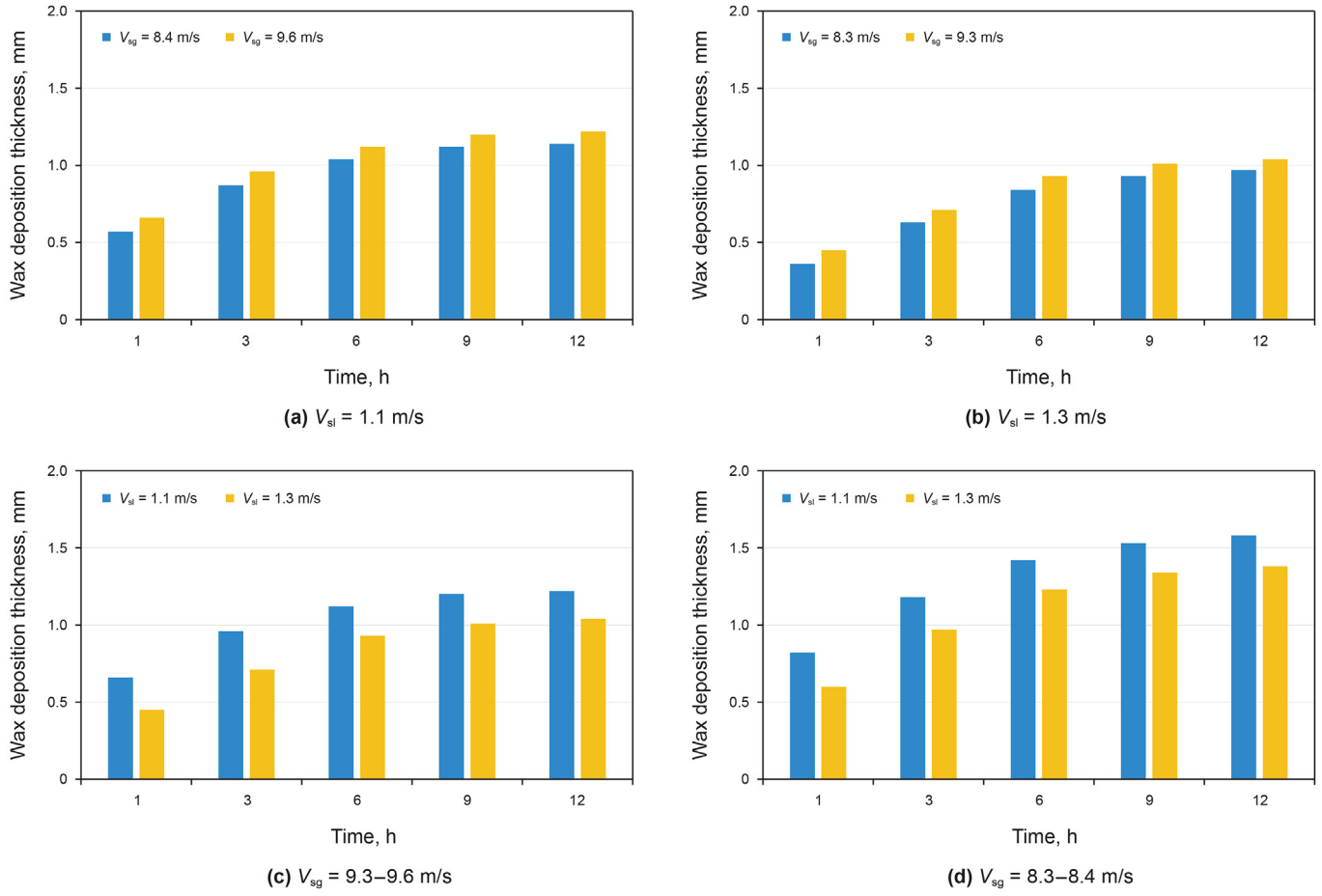

Fig. 6. Summary of deposition thickness at different superficial gas/liquid phase velocities.

Table 1
Calculation results of oil-gas two phase flow parameters.

V_{sl}, m/s	V_{sg}, m/s	Liquid holdup	Actual liquid velocity, m/s	Average wall shear stress, Pa	
				Gas-pipe wall	Liquid film-pipe wall
1.1	8.4	0.23	4.78	0.59	44
	9.6	0.21	5.24	0.51	46
1.3	8.3	0.26	5.00	0.52	52
	9.3	0.24	5.42	0.48	56

phase velocity V_{sg} and a decrease in the liquid holdup H_L will lead to an increase in the actual liquid velocity V_L=V_{sl}/H_L, convective heat transfer, and thermodynamic driving force of wax molecules. Comparing the average wall shear stresses between the liquid film-pipe wall and the gas-pipe wall, it was found that the value of the former was much larger than the latter. The former showed a significant increase as the superficial liquid phase velocity increased, which corresponded to the variation of the actual liquid velocity. Gas phase shear stress changed slightly with varying superficial gas phase velocities, which can be negligible. With the increase of V_{sl}, the shear stress of the liquid film on the pipe wall and the liquid phase shear stripping increased accordingly, which triggered the decrease of the deposition thickness.

To guide the field operations, the wax deposition characteristics of oil-gas two phase with varying gas-oil ratios were described below in terms of total deposition thickness (Fig. 7) and deposition morphology (Fig. 8).

At the same temperature and flow rate, the growth curve of the wax deposition layer with the gas-oil ratio of 0 was positioned farther to above the oil-gas two phase waxy oil. This can be attributed to the fact that the periodic alternating flow of gas and liquid phase reduced the wetting area of the liquid phase, resulting in a smaller wax deposition thickness for both high and medium gas-oil ratios. A comparison of the results from Fig. 7 for the two values of the gas-oil ratios tested showed that the deposited layer was comparatively thicker for the higher gas-oil ratio, due to the higher value of the actual liquid velocity.

In terms of deposition layer morphology, compared with oil-gas two phase, single phase crude oil was in full contact with the pipe wall, and the wax deposition surface was flatter and smoother. While the oil-gas two phase liquid plug/gas core flowed in alternating cycles, the deposition surface was concave and uneven (see Fig. 8 below), was related to the flow pattern characteristics. The bottom and top concave and convex morphologies were contributed by liquid film level fluctuations and alternating gas-liquid plug flow, respectively.

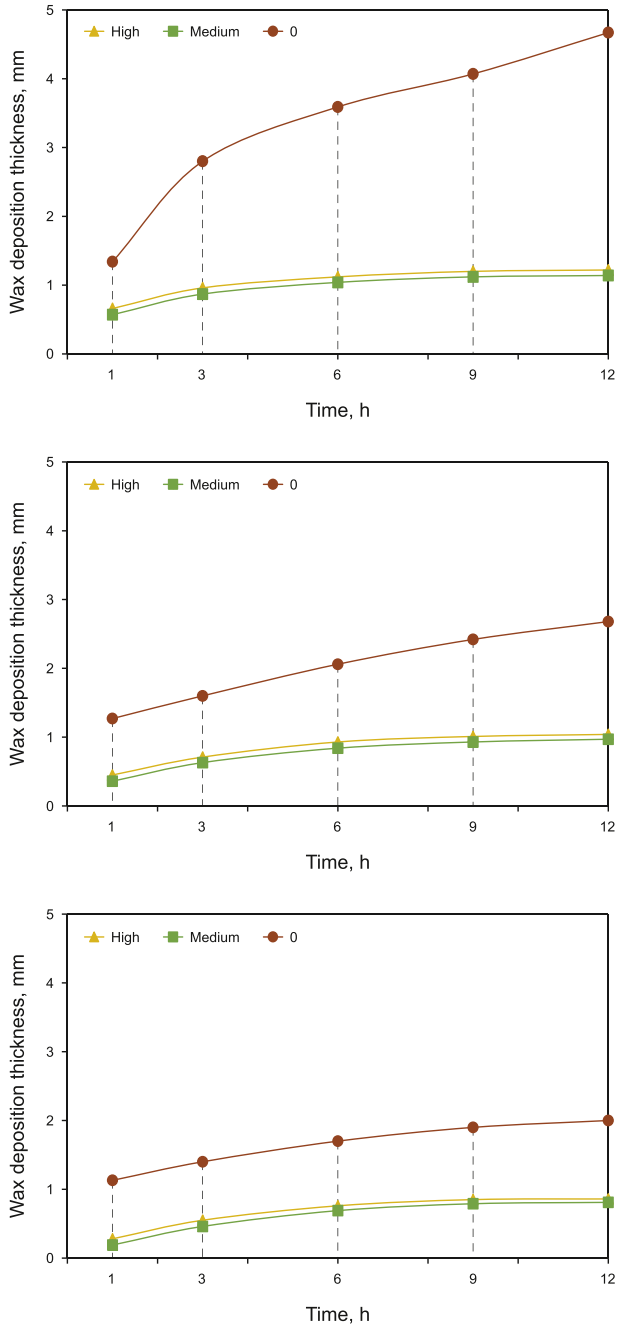

Fig. 7. Wax deposit thickness at different gas-oil ratios.

3.2. Crystal structure of deposition at different circumferential positions

To enrich the feature representations of the deposition layer, we used small angle X-ray scattering (SAXS) experiments to investigate the crystal structure of the wax deposition layer at different circumferential positions. The scattering patterns and wax crystal structure parameters were analyzed for different pipe wall circumferential positions, liquid phase flow rates, and gas-oil ratios.

The scattering intensity profiles of the side and top deposited samples were similar at different circumferential positions of the pipe test sections (red and blue curves in Fig. 9), and their scattering peaks were sharper. While the bottom deposited sample had a broad and low scattering peak (black curve in Fig. 9). It was based, on this evidence, that we suggested that the bottom deposited sample had irregular crystal size and distribution character, which might be caused by the interference of the bottom liquid film area.

By analyzing the small angle scattering curves using the Bragg (1925), Walker and Guinier (1953), Iijima and Strobl (2000), and Porod (1953) theory, some structural parameters such as long period, the radius of gyration, interface layer thickness and fractal dimension could be extracted (Supporting information B). The specific calculation results were shown in Table 2 below.

The bottom deposition layer had a larger long period, gyration radius, fractal dimension, interfacial layer thickness and sheet crystal thickness. It meant that the bottom deposit crystalline micro-areas were widely spaced, large in size, complex in structure, and disordered. In contrast, the electronic density fluctuations value was the smallest, indicating slow thermal motion and hardness of the wax deposition layer.

With the change of liquid phase velocity/flow pattern, the SAXS scattering curve of the bottom deposit layer varies a great deal compared with the top (see Fig. 10). As the flow rate increased, the width of the scattering peak of the bottom deposition increased and the intensity decreased. That is, the increased flow rate disturbed the wax crystal structure of the bottom deposition.

Table 3 showed the comparison of wax crystal structure parameters for the bottom and top deposit layers covering both the laminar and turbulent flow regimes. Changes in the flow rate/pattern can also lead to a significant change in the bottom electronic density fluctuations. For example, the bottom electronic density fluctuations values were 5395.03 and 2004.21 for laminar and turbulent regimes, respectively. However, the top deposition layer electronic density fluctuations value was maintained at around 3000 for different flow regimes. It showed that the bottom deposition changed significantly with the increase of flow velocity, which could give an even higher hardness. As the flow rate increased, the wax crystal long period, gyration radius, fractal dimension and interfacial layer thickness of the bottom deposited layer increased. From a field operations point of view, the SAXS results suggested that bottom deposition in oil-gas two phase should be given sufficient attention.

To analyze the mechanism of gas phase action, comparing the scattering Fig. 11 and Table 4 for single phase and oil-gas two phase deposit samples, it can be seen that the gas phase made the scattering peak intensity weaken, the electronic density fluctuations value decreased, the thermal motion of wax molecules slowed down, and the hardness of wax deposition increased (Sun et al., 2007). In addition, the scattering vector q increased, corresponding to a decrease in the long period. It meant that the spacing between the crystalline microregions of gas-phase initiated deposition decreased. The radius of gyration, fractal dimension and interfacial layer thickness increased under the action of gas phase, which implied an increase in wax crystal size, structural complexity and disordered phases.

The results of the analysis of the electronic density fluctuations value/deposit hardness provided information regarding the introduction of the gas phase, enabling increased the hardness of the wax deposition layer (compared to the single phase), represented by the smaller the value of electronic density fluctuations value. The analysis of the other structural parameters of wax crystals showed that the increase of liquid-phase flow rate and the introduction of gas phase both increased the size of wax crystals, complicated the structure and increased the disordered phases (the increases of gyration radius, fractal dimension and interfacial layer

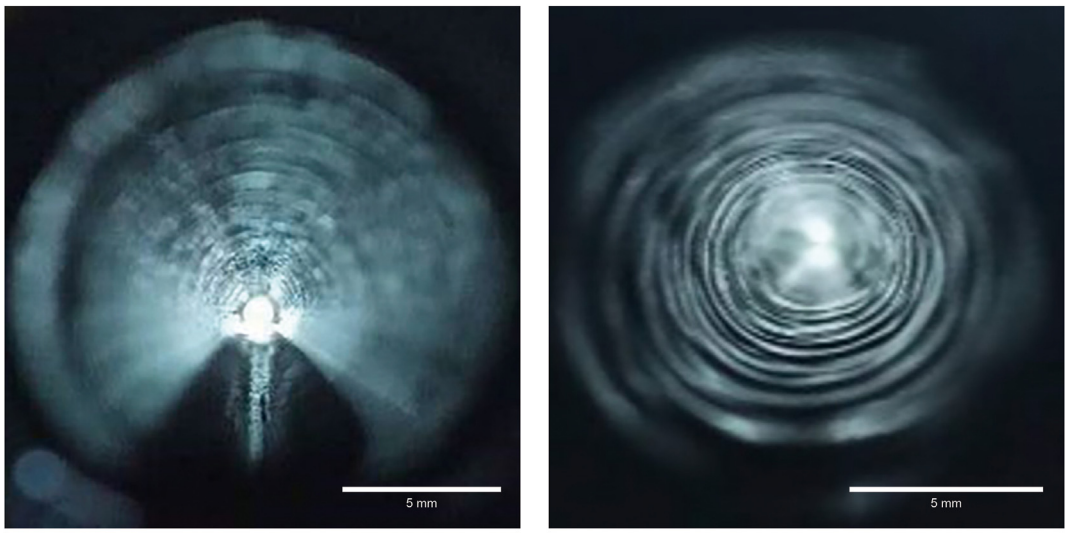

Fig. 8. Comparison of single phase and oil-gas two phase deposition morphology (deposition time 12 h).

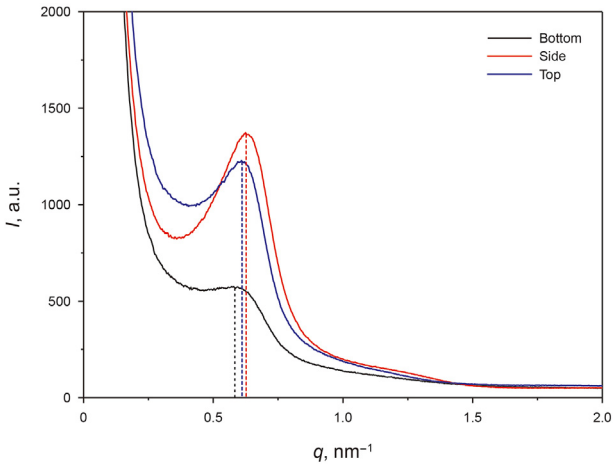

Fig. 9. Scattering intensity curves of oil-gas two phase deposit layers at different annular positions.

thickness), which further confirmed that the actual change of liquid-phase flow rate under the action of gas phase was the dominant mechanism of gas phase action. The increase of the actual liquid velocity under the action of gas phase could promote the entanglement and aggregation of wax molecules, which made an increase in the size of wax crystals and also interfered with the crystallization of wax molecules, and complicated the crystal structure.

4. Conclusions

(1) The wax deposition thickness of oil-gas two phase within 12 h increased with increasing oil temperature at three oil temperatures of 40, 45 and 50 °C for low velocity laminar flow, high velocity laminar flow and turbulent flow. The oil temperature increased and the temperature difference between the oil flow and wall surface increased, leading to an increase in the wax molecular diffusion driving force and thus the deposition thickness. That is, the oil-gas two phase deposition was still consistent with the molecular diffusion mechanism.

(2) In the range of experimental gas/liquid phase superficial velocities (V_{sl} = 1.1, 1.3 m/s, V_{sg} = 8.3–8.4, 9.3–9.6 m/s), the wax deposition thickness of oil-gas two phase tended to increase with the increase in the value of V_{sg}. But as the value of V_{sl} increased, the results indicated that the wax deposition thickness of oil-gas two phase decreased. By combining the above experimental results with the oil-gas two phase flow characteristics parameters, the analysis revealed that the enhanced convective heat transfer (actual liquid velocity) and the increase in shear stripping (shear stress between liquid film and pipe wall) brought by V_{sg} and V_{sl} were the main influencing mechanisms.

(3) Among the three gas-oil ratios, we will get a large deposition thickness when the gas-oil ratio was equal to 0. The deposition thickness at medium (7) and high (15) gas-oil ratios was lower than that at 0 gas-oil ratio. There were no discernible deposition thickness differences between medium and high gas-oil ratios. Further, a careful observation

Table 2
Wax crystal structure of oil-gas wax deposition layer (different radial positions).

	Scattering vector q	Long period L	Gyration radius R_g	Fractal dimension α	Interface layer thickness σ	Electronic density fluctuations
Bottom	0.58916	10.66	14.55	2.22	1.01	2004.21
Side	0.62624	10.03	14.04	2.07	0.79	3145.08
Top	0.61063	10.28	13.70	1.98	0.79	3120.21

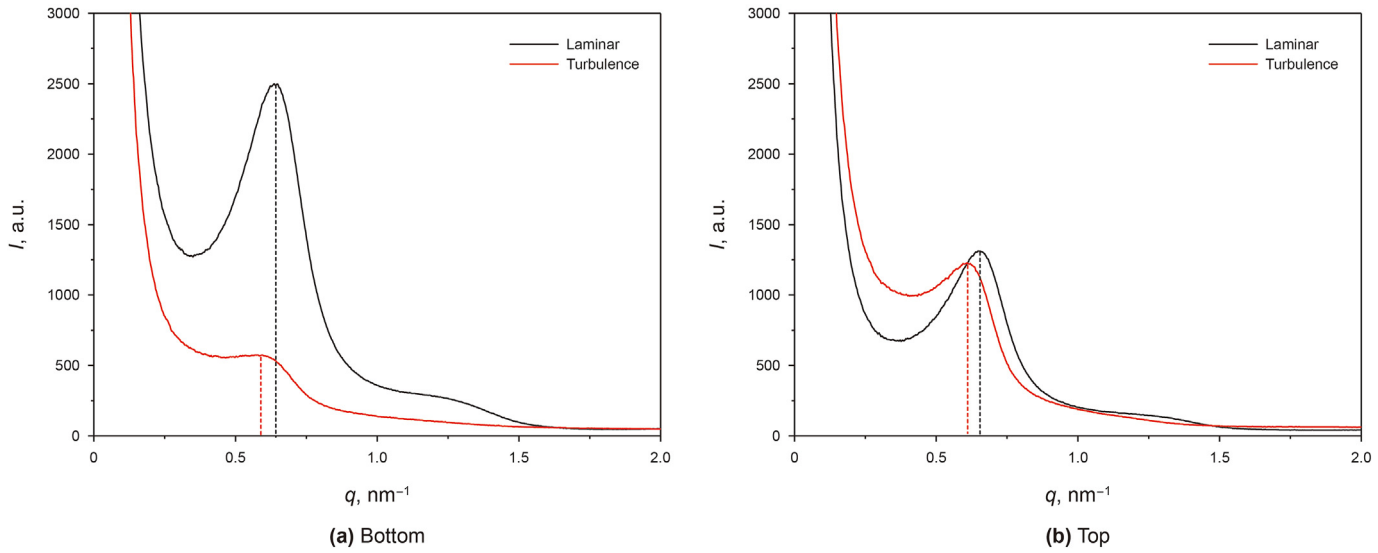

Fig. 10. Scattering intensity curves of oil-gas two phase deposit layers in different flow regimes.

Table 3
Wax crystal structure of oil-gas wax deposition layer (different flow rates/flow patterns).

		Scattering vector q	Long period L	Gyration radius R_g	Fractal dimension α	Interface layer thickness σ	Electronic density fluctuations
Bottom	Laminar	0.64185	9.78	13.39	1.88	0.83	5395.03
	Turbulence	0.58916	10.66	14.55	2.22	1.01	2004.21
Top	Laminar	0.65551	9.58	14.27	2.14	0.89	3021.03
	Turbulence	0.61063	10.28	13.70	1.98	0.79	3120.21

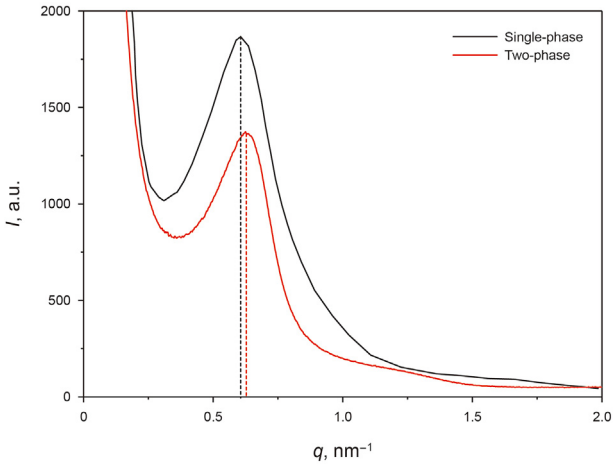

Fig. 11. Scattering intensity curves of single phase and oil-gas two phase deposit layers.

demonstrated that the wax deposition thickness was slightly larger at high gas-oil ratios, which was related to the variation of actual liquid velocity. In summary, the apparent characteristics of the oil-gas two phase deposition layer were a periodic alternating flow of gas and liquid phases, which made the wetting area of the liquid phase reduced and the deposition surface uneven.

(4) The results of the crystal structure of the deposition layers under SAXS experiments showed that the crystalline microregions of the bottom deposition were widely spaced, large in size, complex in structure and disordered phases in different circumferential positions. The variation of liquid velocity had a great influence on the wax crystal structure of bottom deposition. Meanwhile, the analysis of electronic density fluctuations (wax deposition hardness) showed that there was a maximum hardness in the bottom deposition layer. Oil-gas two phase wax deposition at the bottom should be given sufficient attention in field pipelines transporting waxy crude oils.

CRediT authorship contribution statement

Chuan-Shuo Wang: Writing – original draft. **Qian-Li Ma:** Methodology. **Xiao-Fang Lv:** Writing – review & editing. **Jie Zhang:** Investigation. **Yang Liu:** Conceptualization. **Shi-Dong Zhou:** Supervision.

Table 4
Wax crystal structure of single phase and oil-gas two phase wax deposition.

	Scattering vector q	Long period L	Gyration radius R_g	Fractal dimension α	Interface layer thickness σ	Electronic density fluctuations
Single phase	0.60033	10.46	13.87	1.79	0.72	4862.67
Two phase	0.62624	10.03	14.04	2.07	0.79	3145.08

Declaration of competing interest

The authors declare that they have no known competing financial interests or personal relationships that could have appeared to influence the work reported in this paper.

Acknowledgments

This work was supported by the National Natural Science Foundation of China (Grant No. 52274061 & 52004039 & 51974037), China Postdoctoral Science Foundation (Grant No. 2023T160717 & 2021M693908), CNPC Innovation Found (Grant No.2022DQ02-0501), Changzhou Applied Basic Research Program (Grant No. CJ20230030), The major project of universities affiliated with Jiangsu Province basic science (natural science) research (Grant No.21KJA440001), Jiangsu Qinglan Project, Changzhou Longcheng Talent Plan - Youth Science and Technology Talent Recruitment Project.

Appendix A. Supplementary data

Supplementary data to this article can be found online at https://doi.org/10.1016/j.petsci.2024.01.003.

References

Aiyejina, A., Chakrabarti, D.P., Pilgrim, A., et al., 2011. Wax formation in oil pipelines: a critical review. Int. J. Multiphas. Flow 37 (7), 671–694. https://doi.org/10.1016/j.ijmultiphaseflow.2011.02.007.

Bragg, W., 1925. X Rays and Crystal Structure, fifth ed. The Scientific Monthly.

Cai, J.M., Zhang, G.Z., 2003. Determination of wax deposite thickness in model loop with differential pressure method. J. Univ. Petrol., China 6, 68–71.

Chi, Y.D., Sarica, C., Daraboina, N., 2019. Experimental investigation of two-phase gas-oil stratified flow wax deposition in pipeline. Fuel 247, 113–125. https://doi.org/10.1016/j.fuel.2019.03.032.

Dong, B., Sheng, W., Yang, H., et al., 1997. Status of the small-angle scattering station at the Beijing synchrotron radiation facility. J. Appl. Crystallogr. 30, 877–879. https://doi.org/10.1107/S002188989700160X.

Duan, J.M., Deng, S.S., Xu, S., et al., 2018. The effect of gas flow rate on the wax deposition in oil-gas stratified pipe flow. J. Pet. Sci. Eng. 162, 539–547. https://doi.org/10.1016/j.petrol.2017.10.058.

Duan, J.M., Liu, H.S., Jiang, J.Z., et al., 2017. Numerical prediction of wax deposition in oil-gas stratified pipe flow. Int. J. Heat Mass Transf. 105, 279–289. https://doi.org/10.1016/j.ijheatmasstransfer.2016.09.082.

Fan, K.F., Li, S., Li, R.B., 2021. Development of wax molecular diffusivity correlation suitable for crude oil in wax deposition: experiments with a cold-finger apparatus. J. Pet. Sci. Eng. 205, 12. https://doi.org/10.1016/j.petrol.2021.108851.

Gong, J., Zhang, Y., Liao, L.L., et al., 2011. Wax deposition in the oil/gas two-phase flow for a horizontal pipe. Energy Fuels 25 (4), 1624–1632. https://doi.org/10.1021/ef101682u.

Gouze, B., Nardin, T., Diat, O., et al., 2019. Aggregation of semifluorinated alkanes in cyclic organic solvents: a SAXS study. Colloid Interface Sci. Commun. 31, 100189. https://doi.org/10.1016/j.colcom.2019.100189.

Huang, H.R., Wang, W., Peng, Z.H., et al., 2018. The influence of nanocomposite pour point depressant on the crystallization of waxy oil. Fuel 221, 257–268. https://doi.org/10.1016/j.fuel.2018.01.040.

Iijima, M., Strobl, G.J.M., 2000. Isothermal crystallization and melting of isotactic polypropylene analyzed by time-and temperature-dependent small-angle X-ray scattering experiments. Macromolecules 33 (14), 5204–5214. https://doi.org/10.1016/j.polymer.2005.03.107.

Leporini, M., Terenzi, A., Marchetti, B., et al., 2019. Experiences in numerical simulation of wax deposition in oil and multiphase pipelines: theory versus reality. J. Pet. Sci. Eng. 174, 997–1008. https://doi.org/10.1016/j.petrol.2018.11.087.

Li, Z., Li, Z., Li, D., et al., 2019. A small sample stretcher for in-situ small angle X-ray scattering measurement. J. Instrum. 14, T05002. https://doi.org/10.1088/1748-0221/14/05/t05002.

Li, Z.H., Wu, Z.H., Mo, G., Xing, et al., 2014. A small-angle x-ray scattering station at beijing synchrotron radiation facility. Instrum. Sci. Technol. 42 (2), 128–141. https://doi.org/10.1080/10739149.2013.845845.

Liu, Z.M., Li, Y.X., Wang, W.C., et al., 2020. Wax and wax-hydrate deposition characteristics in single-, two-, and three-phase pipelines: a review. Energy Fuels 34 (11), 13350–13368. https://doi.org/10.1021/acs.energyfuels.0c02749.

Matzain, A., Apte, M.S., Zhang, H.Q., et al., 2002. Investigation of paraffin deposition during multiphase flow in pipelines and wellbores part 1: experiments. J. Energy Resour. Technol. 124 (3), 180–186. https://doi.org/10.1115/1.1484392.

Porod, G., 1953. X-ray and light scattering by chain molecules in solution. J. Polymer Science 10 (2), 157–166. https://doi.org/10.1002/pol.1953.120100203.

Quan, Q., Ran, W., Yang, L., et al., 2018. The effect of pressure on wax deposition from wax-solvent mixtures with natural gas. J. Pet. Sci. Eng. 171, 1318–1325. https://doi.org/10.1016/j.petrol.2018.08.040.

Quan, Q., Wang, S.X., Sun, N.N., et al., 2020. Experimental study on wax deposition of gas-liquid under intermittent flow. Pet. Sci. Technol. 38 (4), 331–337. https://doi.org/10.1080/10916466.2019.1705854.

Rittirong, A., Panacharoensawad, E., Sarica, C., 2017. Experimental study of paraffin deposition under two-phase gas/oil slug flow in horizontal pipes. SPE Prod. Oper. 32 (1), 99–117. https://doi.org/10.2118/184386-pa.

Singh, A., Panacharoensawad, E., Sarica, C., 2017. A mini pilot-scale flow loop experimental study of turbulent flow wax deposition by using a natural gas condensate. Energy Fuels 31 (3), 2457–2478. https://doi.org/10.1021/acs.energyfuels.6b02125.

Singh, P., Venkatesan, R., Fogler, H.S., et al., 2000. Formation and aging of incipient thin film wax-oil gels. AIChE J. 46 (5), 1059–1074. https://doi.org/10.1002/aic.690460517.

Sun, M., Mou, H., Wang, Y., et al., 2007. SAXS observation of structural evolution of heated olefin. Nucl. Tech. 30 (7), 568–570.

Van der Geest, C., Guersoni, V.C.B., Merino-Garcia, D., et al., 2018. Wax deposition experiment with highly paraffinic crude oil in laminar single-phase flow unpredictable by molecular diffusion mechanism. Energy Fuels 32 (3), 3406–3419. https://doi.org/10.1021/acs.energyfuels.8b00269.

Walker, C.B., Guinier, A.J.A.M., 1953. An X-ray investigation of age hardening in alag. Acta Metall. 1 (5), 568–577. https://doi.org/10.1016/0001-6160(53)90087-X.

Yu, X., Gao, Y.H., Cai, D.J., et al., 2021. Wax deposition law under a gas-liquid bubbly flow pattern. ACS Omega 6 (36), 23015–23022. https://doi.org/10.1021/acsomega.0c04911.

Zhang, H.Q., Sarica, C., 2011. A model for wetted-wall fraction and gravity center of liquid film in gas/liquid pipe flow. SPE J. 16 (3), 692–697. https://doi.org/10.2118/148330-pa.